Experimental and simulation analysis of carrier lifetimes in GaAs/AlGaAs Avalanche Photo–Diodes

F. Driussi[1], A. Pilotto[1], D. De Belli[1], M. Antonelli[2], F. Arfelli[3,4], G. Biasiol[5], G. Cautero[2,4], R. H. Menk[2,4,6], C. Nichetti[2,3], L. Selmi[6], T. Steinhartova[3,5] and P. Palestri[1]
[1]DPIA, Università degli Studi di Udine, Udine, Italy, Email: francesco.driussi@uniud.it
[2]Elettra–Sincrotrone Trieste S.C.p.A, Area Science Park Basovizza, Trieste, Italy
[3]Università di Trieste, Department of Physics, Trieste, Italy
[4]Istituto Nazionale di Fisica Nucleare, INFN Sezione di Trieste, Trieste, Italy
[5]IOM CNR, Laboratorio TASC, Area Science Park Basovizza, Trieste, Italy
[6]University of Saskatchewan, Department of Medical Imaging, Saskatoon, Canada
[7]Università di Modena e Reggio Emilia, Modena, Italy

***Abstract*—Extensive experimental characterization and TCAD simulation analysis have been used to study the dark current in Avalanche Photo–Diodes (APDs). The comparison between the temperature dependence of measurements and simulations points out that SRH generation/recombination is responsible for the observed dark current. After the extraction of the carrier lifetimes in the GaAs layers, they have been used to predict the APD collection efficiency of the photo–generated currents under realistic operation conditions and as a function of the photo–generation position inside the absorption layer.**

I. Introduction

New applications in the field of bio–medical instruments push nowadays the development of new sensors with improved performance. Next generation X–rays detectors require higher count rate and higher quantum efficiency for medium and high photon energy. Avalanche photo–diodes (APDs) in III–V compounds are very promising with respect to silicon ones thanks to the higher atomic number of the material that allows for thinner detectors and to the larger band–gap that limits the leakage current [1], [2]. However, the APD development and optimization requires an in–depth understanding of the physical mechanisms involved in the device operation [3].

The dark current in APDs is a major concern since it limits the signal–to–noise ratio (SNR). It originates from generation/recombination processes that also reduce the number of photo–generated carriers able to reach the multiplication region, further reducing SNR. In this work, we characterized in temperature the dark current of GaAs/AlGaAs based APDs, aiming to investigate its origin and to extract relevant parameters related to the carrier generation/recombination. TCAD simulations have been exploited to obtain the carrier lifetimes and to predict the collection efficiency of the photo–generated carriers.

II. Device structure

The structure of the fabricated APDs is sketched in Fig. 1(a). The intrinsic 4.5 μm GaAs absorption layer (where photo–generation takes place) is sandwiched between the top $p+$ contact and a p–doped, two–dimentional (δ) layer, that separates the absorption and multiplication regions. This latter is made of 12 repetitions of a stack with a 35nm GaAs layer, a 25nm $Al_{0.45}Ga_{0.55}As$ film and 20 nm of a linearly graded alloy with an Al content that is increased from 1% to 45% [1]. The resulting *staircase* multiplication region features a periodically modulated conduction band profile [see Fig. 1(b)] [6], that boosts the impact ionization of electrons, thus allowing a large signal multiplication with a good SNR [1], [7].

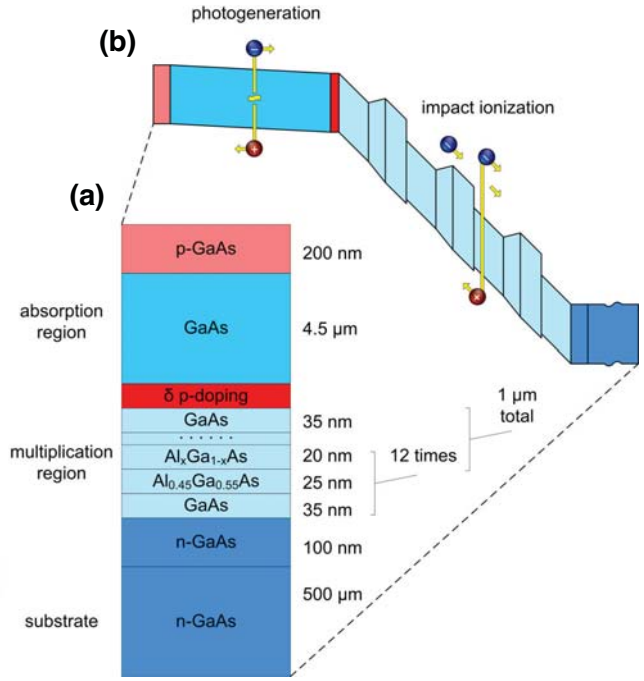

Fig. 1. (a) Sketch depicting the layered stack of the fabricated APDs and also highlighting the absorption and multiplication regions of the device. (b) Energy band profiles along the device depth under an applied reverse bias V_{REV}. The energy step between the conduction band minima of $Al_{0.45}Ga_{0.55}As$ and GaAs is 0.355 eV in the performed simulations [4], [5]. Photo–generated electrons are multiplied by the impact ionization events taking place inside the *staircase* multiplication region.

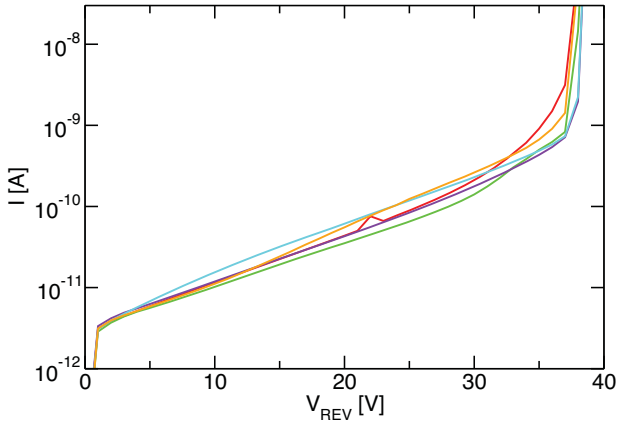

Fig. 2. Dark current versus reverse voltage V_{REV} for a subset of APDs representative of the fabrication technology. Breakdown voltage of the devices is around 38 V.

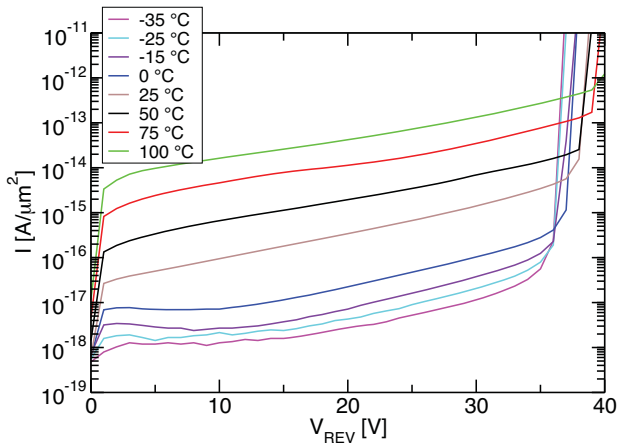

Fig. 3. Experimental IV curves of a representative APD for different operation temperatures T. Lowering the temperature, the dark current largely decreases, together with the breakdown voltage.

III. Experimental Characterization

The APDs are measured as a function of the reverse bias (V_{REV}). Fig. 2 reports the current–voltage (IV) curves of a subset of the measured APDs that can be considered as representative of the fabrication process. It is worth mentioning that the currents scale with the device area (not shown), so border effects may be excluded. Then the IV curves of the APDs are measured over temperature (T, Fig. 3); as it can be seen, the dark current is largely modulated by T. Also the breakdown voltage (V_{BK}, see also Fig. 4) increases with T, confirming the avalanche multiplication process at the base of the APD operation.

For given V_{REV} values, Fig. 5 reports the Arrhenius plots of the current (symbols). These curves essentially follow the exponential Arrhenius law

$$I = A \exp\left(-\frac{E_A}{kT}\right), \qquad (1)$$

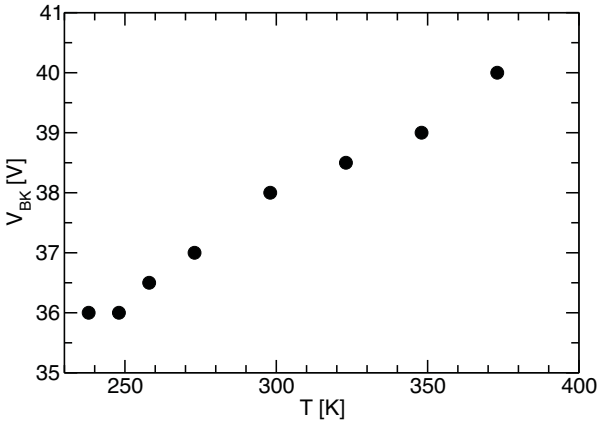

Fig. 4. Breakdown voltage versus T curve: the positive temperature coefficient confirms the avalanche multiplication process.

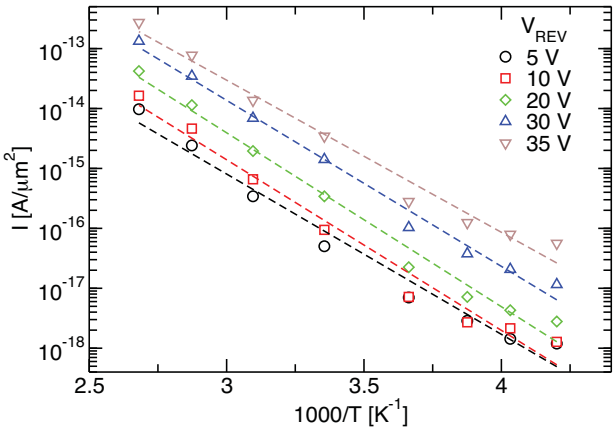

Fig. 5. Arrhenius plots of the dark current for several V_{REV} values. Curves show linear behavior down to low temperatures where they start to deviate likely because a temperature independent component enters into play.

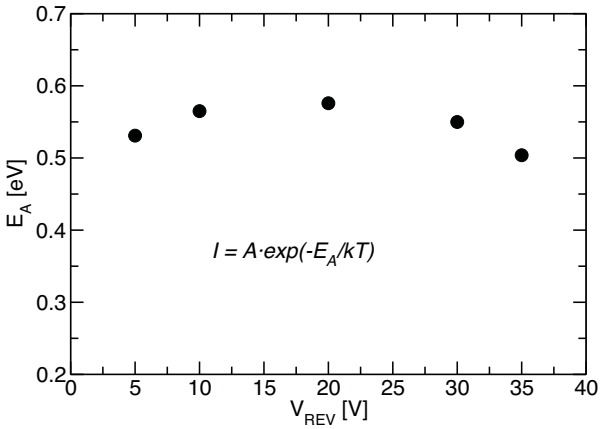

Fig. 6. Activation energy extracted from the Arrhenius plots in Fig. 5. E_A is rather independent of the selected V_{REV} value.

where k is the Boltzmann constant. Thus, these data are used to extract the activation energy E_A (Eq. 1). The extracted E_A is reported in Fig. 6 and it results to be quite independent

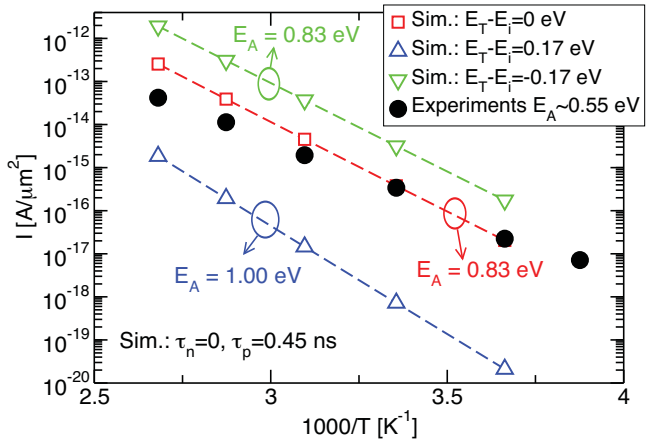

Fig. 7. Arrhenius plots simulated for $V_{REV} = 20$ V assuming fixed τ_n and τ_p and variable trap energy depth E_T. For constant τ_n and τ_p, simulations cannot reproduce the measurements. Simulated E_A is always larger than in experiments. E_i is the Fermi level in the intrinsic semiconductor.

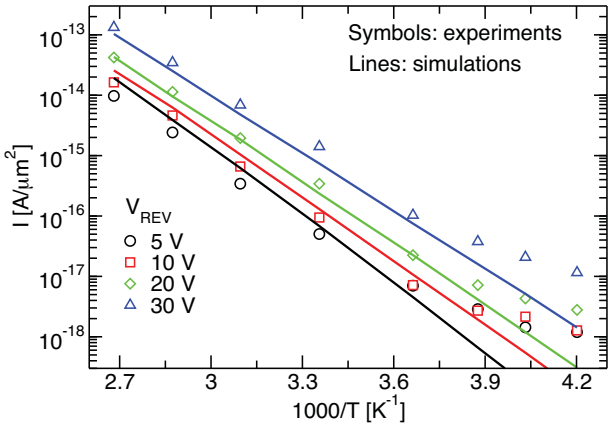

Fig. 8. Arrhenius plots simulated with $\tau_n = \tau_p$ as in Eq. 5 and with $E_T = E_i$. Simulations now reproduce the experiments for different V_{REV}. A power-law temperature dependence is assumed to model the lifetimes (Eq. 5, $\tau_{300K} = 0.39$ ns, $\alpha = 6.06$). At low T, the experiments deviate from the linear behavior most likely because of the arise of a temperature independent component not included in simulations.

of V_{REV}, with a value of about 0.55 eV, that suggests that the dark current is related to traps in the band–gap of the III–V alloy, like in the Shockley Read Hall (SRH) process. Furthermore, since E_A does not depend on the bias (i.e. on the electric field), effects like the band–to–band tunneling (BBT) are ruled out.

IV. Simulations and Discussion.

The commercial TCAD Sentaurus is used to reproduce the dependence on T and V_{REV} of the APD currents [8]. In the simulator, the SRH generation/recombination rate (U_{SRH}) is modeled through the following set of equations:

$$U_{SRH} = R - G = \frac{np - n_i^2}{\tau_p(n + n_1) + \tau_n(p + p_1)}, \quad (2)$$

$$n_1 = n_i \exp\left(\frac{E_T - E_i}{kT}\right), \quad (3)$$

$$p_1 = n_i \exp\left(-\frac{E_T - E_i}{kT}\right), \quad (4)$$

where τ_n and τ_p are the electron and hole lifetimes, respectively and E_T is the trap energy depth. E_i and n_i are, instead, the Fermi level and the electron density of the intrinsic semiconductor, respectively.

A. Simulation of the dark current

Figure 7 reports the simulation analysis we performed on the current versus T data at $V_{REV} = 20$ V. We can reproduce the experiments at 300 K (i.e. $1000/T = 3.33$ K^{-1}) by setting $\tau_n = 0$ and $\tau_p = 0.45$ ns and by assuming $E_T = E_i$ (red dashed line). However, we obtain $E_A = 0.83$ eV that is larger than in the experiments.

With $\tau_n = 0$, the slope of the Arrhenius plot can be eventually modulated by changing E_T with respect to E_i (see Eqs. 2–4). Indeed, for $(E_T - E_i) > 0$, the slope of the simulated curve actually changes (Fig. 7, blue line), but E_A increases. Instead, for $(E_T - E_i) < 0$, E_A does not change

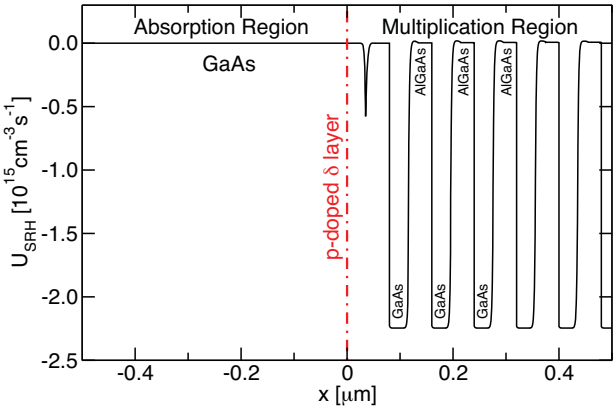

Fig. 9. SRH generation/recombination function along the device depth. $x = 0$ corresponds to the p–doped δ layer position that separates the absorption and multiplication regions. Note that carrier generation occurs in the GaAs layers of the multiplication region. $V_{REV} = 20$ V.

(green line). This is because, in the generation/recombination function (Eq. 2), n_1 becomes negligible with respect to the electron density n (see Eq. 3). A similar behavior is observed with $\tau_n \neq 0$ and $\tau_p = 0$ or $\tau_n = \tau_p$: the U_{SRH} value required to reproduce the experiments always leads to $E_A \geq 0.83$ eV, hence to E_A values much larger than experimentally observed.

In summary, Fig. 7 indicates that the experiments can be reproduced only by assuming temperature dependent carrier lifetimes. Therefore, we assume $E_T = E_i$ and equal τ_n and τ_p values with a power–law dependence on T as in [8], [9], [10]:

$$\tau_n = \tau_p = \tau_{300K} \cdot \left(\frac{T}{300}\right)^{\alpha}, \quad (5)$$

where τ_{300K} is the carrier lifetime at 300 K.

Now, by using $\tau_{300K} = 0.39$ ns and $\alpha = 6.06$ in Eq. 5, the simulations in Fig. 8 reproduce well the experimental Arrhenius plots at different V_{REV}, with E_A values close to

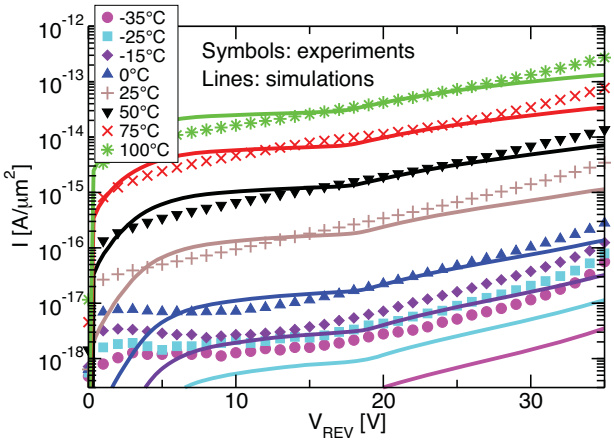

Fig. 10. Simulated IV curves with $\tau_n = \tau_p$ as in Eq. 5. Simulations well reproduce the experiments, except at low T, when a temperature independent component most likely arises in the measurements.

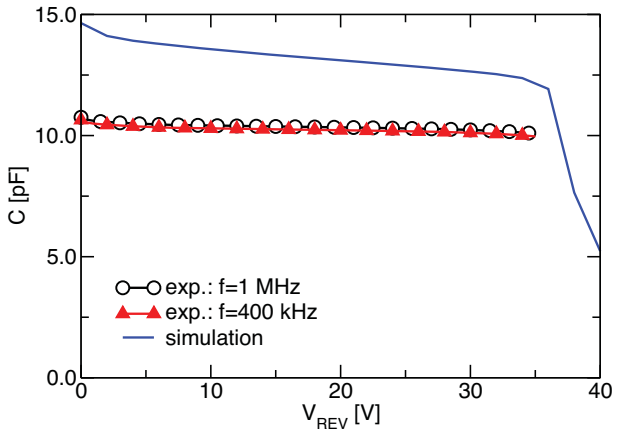

Fig. 11. Typical experimental capacitance–voltage curves (symbols) of the measured APDs. The TCAD simulation (line) is reported for comparison. The agreement is limited mostly because we simulated the APD with nominal dimensions and with nominal parameters for the materials. A better agreement can be found by tuning the parameters of the structure. It is worth noting that the simulation predicts that the depletion of the absorption region occurs for $V_{REV} > 35$ V.

those in Fig. 6. The obtained positive α value agrees with [9]. Notice that, in the simulations, the absorption region is always at equilibrium, thus we are only able to extract the lifetimes for the GaAs layers in the multiplication region where the SRH generation/recombination mostly occurs (see Fig. 9).

This parameter set allows us to fit the IV curves at different T (Fig. 10). The agreement between experiments and simulations is good down to $T = -15$ °C. At lower temperatures, a T independent component of the current may arise in the measurements. Furthermore, the limited agreement for very small V_{REV} is most likely due to the fact that in the simulations we consider: 1) the nominal APD structure; 2) uniform trap density (i.e. lifetimes) along the multiplication region. Concerning the first point, Fig. 11 reports the experimental capacitance–voltage (CV) curves of a typical APD (symbols) and the CV calculated considering nominal dimensions and

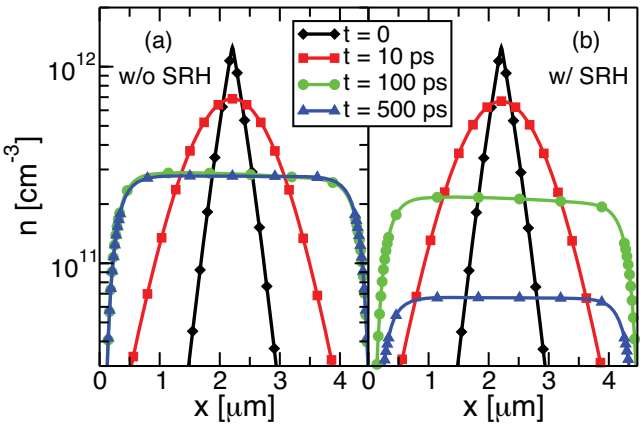

Fig. 12. Electron density n calculated in absorption layer at different instants (t) after the generation of an electron–hole pair (in the middle). After the generation, carrier diffuse all over the absorption layer, due to the negligible electric field in the region. Then, without the SRH process (a), electrons can exits the region only through the multiplication layer (towards the right). Instead, with SRH (b), electrons partly recombine before reaching the multiplication layer. Area of the device is 1 μm^2.

nominal parameters for the materials in the simulated structure. The mismatch between simulated and measured CV curves suggests that better agreement between the model and the experiments in both Figs. 10 and 11 may be obtained by tuning the simulated APD geometry/composition.

Moreover, a larger trap density near the δ layer (it may be source of defects) can induce a larger current also when the multiplication region is not fully depleted, thus resulting in a larger dark current at low V_{REV}.

B. Simulation of the collection efficiency

We have also simulated the response of the APD to the photo–generation of an electron–hole pair in a position corresponding to the middle of the absorption layer. In this simulation, we applied $V_{REV} = 28$ V, a voltage at which the carrier multiplication starts in the APD, but it is not large enough to make the electric field penetrate into the absorption region [1]. This is confirmed by the CV curves in Fig. 11, showing that up to $V_{REV} = 35$ V, the δ layer confines the voltage drop into the multiplication region and no capacitance drop is seen [1]. Indeed, only for $V_{REV} > 35$ V the simulation predicts that the electric field penetrates also into the absorption region causing the capacitance drop (Fig. 11, dashed line).

In this respect, Fig. 12 shows how, after the generation of the electron–hole pair in the middle of the absorption layer, the charge diffuses all over the region because of the negligible electric field in the layer, leading to a rather flat electron density (n) after some time (t). Then, without considering the SRH generation recombination [Fig. 12(a)], electrons can exit the device only through the multiplication layer that is located at the right of the absorption layer ($x > 4.5$ μm).

Figure 12(b) shows, instead, that when including the SRH process, electrons may recombine inside the absorption layer before reaching the multiplication region (compare circle and triangles), thus reducing the number of carriers that are finally

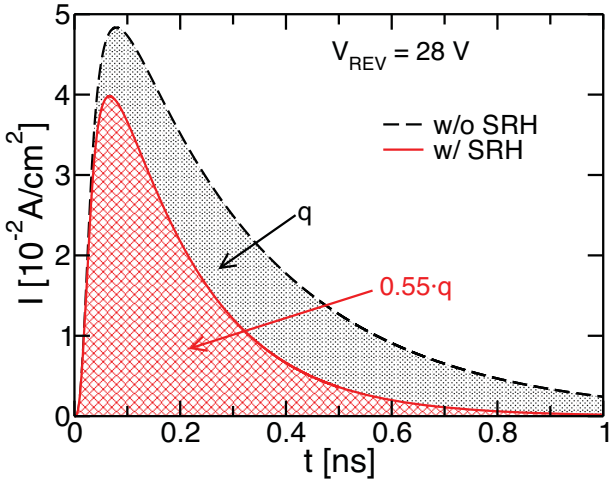

Fig. 13. Simulated current collected at the n–type contact as a function of time after the generation of an electron–hole pair in the middle of the absorption layer. The current is simulated including (red) or not (black) the SRH generation/recombination. At $V_{REV} = 28$ V, the SRH process causes the loss of 45% of the photo–generated charge.

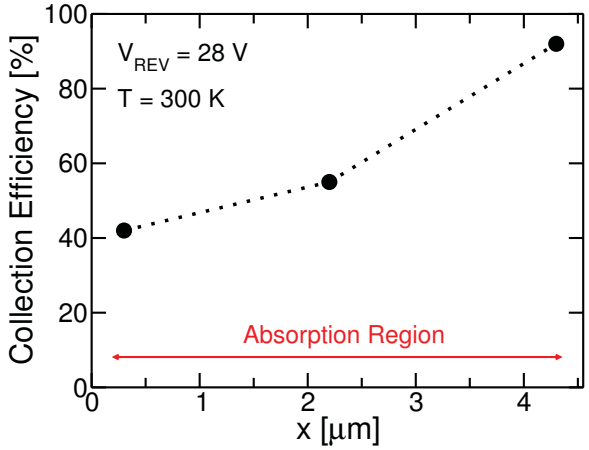

Fig. 14. Collection efficiency as a function of the position inside the absorption layer where the photo–generation take place. If the electron–hole pair is generated closer to the multiplication region ($x > 4.5$ μm), the collection efficiency is larger.

collected at the n–type contact of the device and, hence, lowering the sensitivity of the APD to the electron–hole pair generation event.

To better illustrate this point, Fig. 13 reports the simulated current waveform at the n–type contact after the electron–hole pair generation: without the SRH recombination all the charge exits the device (black line), and the current integral over time gives exactly the photo–generated charge. Instead, when SRH is active inside the device, only the 55% of the charge reaches the contact (red line); therefore the SRH recombination causes the loss of about the 45% of photo–generated charge. Note that, for this calculations, we assumed the same carrier lifetimes in the GaAs absorption region and in the GaAs layers of the multiplication region.

Of course, the probability to recombine for a photo–generated electron depends also on how long it has to travel to reach the APD contact and, hence, on the position at which it is generated inside the absorption region. To verify this, in Fig. 14, we calculated the collection efficiency as a function of the photo–generation position. As expected, the closer to the multiplication region the photo–generation is, the larger the collection efficiency of the APD is, because of the reduction of the recombination probability. The collection efficiency is 42% when electrons are generated near the p–contact (left), while it is 92% for a generation close to the δ layer (right).

V. Conclusion

Experiments and TCAD simulations allowed us to extract the SRH carrier lifetimes in GaAs/AlGaAs APDs. These values were used for calibrated simulations of the collection efficiency of the photo–generated current under realistic operating conditions.

The results show that the collection efficiency goes from a minimum of 42%, for a photo–generation near the top contact of the device, to a maximum value of 92% when the electron–hole pair is generated at the end of the absorption layer, hence near the multiplication layer.

These collection efficiency is in general quite high, thus reassuring on the sensitivity of the studied APDs. However, the large collection efficiency dependence on the position inside the absorption layer of the photo–generation rises questions concerning the potential energy resolution of these photo–detectors. It is of course a fact that, to collect high energy particles, absorption layers with not very small thickness are required and, thus, the distribution of the photo–generation events along the device may become a concern for these APDs.

Acknowledgment

The work was funded by the Italian MIUR through the PRIN 2015 Project under Grant 2015WMZ5C8.

References

[1] T. Steinhartova, C. Nichetti, M. Antonelli, G. Cautero, R.H. Menk, A. Pilotto, F. Driussi, P. Palestri, L. Selmi, K. Koshmak, S. Nannarone, F. Arfelli, S. Dal Zilio and G. Biasiol, "Influence of p-doping on the behaviour of GaAs/AlGaAs SAM-APDs for synchrotron radiation", *Journal of Instrumentation*, vol. 12, C11017, 2017, DOI: 10.1088/1748-0221/12/11/C11017.

[2] C. Nichetti, T. Steinhartova, M. Antonelli, G. Cautero, R. H. Menk, A. Pilotto, F. Driussi, P. Palestri, L. Selmi, F. Arfelli, and G. Biasiol, "Gain and noise in GaAs/AlGaAs avalanche photodiodes with thin multiplication regions", *Journal of Instrumentation*, vol. 14, C01003, 2019, DOI: 10.1088/1748-0221/14/01/C01003.

[3] A. Pilotto, C. Nichetti, P. Palestri, L. Selmi, M. Antonelli, F. Arfelli, G. Biasiol, G. Cautero, F. Driussi, D. Esseni, R. H. Menk, T. Steinhartova, "Optimization of GaAs/AlGaAs staircase avalanche photodiodes accounting for both electron and hole impact ionization", *Solid State Electronics*, in press, DOI: 10.1016/j.sse.2019.107728

[4] M.-K. Tsai, Y.-J. Yang, Y.-W. Wu, S.-W. Tan, W.-S. Lour, "Improvements in direct-current characteristics of $Al_{0.45}Ga_{0.}55As$/GaAs digital–graded superlattice–emitter HBTs with reduced turn–on voltage by wet oxidation", *IEEE Transactions on Electron Devices* , vol. 50, pp. 303–309, 2003.

[5] V. Spagnolo, G. Scamarcio, W. Schrenk, and G. Strasser, "Influence of the band-offset on the electronic temperature of GaAs/Al(Ga)As superlattice quantum cascade lasers", Semiconductor Science and Technology, vol. 19, pp. S110–S112, 2004.

[6] F. Capasso, W. T. Tsang, and G. F. Williams, “Staircase solid-state photomultipliers and avalanche photodiodes with enhanched ionization rates ratio,” *IEEE Transaction on Electron Devices*, vol. 30, no. 4, pp. 381–390, Apr. 1983, DOI: 10.1109/T-ED.1983.21132.

[7] C. Nichetti, A. Pilotto, P. Palestri, L. Selmi, M. Antonelli, F. Arfelli, G. Biasiol, G. Cautero, F. Driussi, N. Y. Klein, R. H. Menk, and T. Steinhartova, “An Improved Nonlocal History–Dependent Model for Gain and Noise in Avalanche Photodiodes Based on Energy Balance Equation”, *IEEE Transaction on Electron Devices*, vol. 65, pp. 1823–1829, 2018, DOI: 10.1109/TED.2018.2817509.

[8] *Sentaurus Device User Guide, Version L_2016.03*, Synopsys, Mountain View, CA, USA, 2016.

[9] H. Goebel, K. Hoffmann, “Full dynamic power diode model including temperature behavior for use in circuit simulators”, *Proc. of International Symposium on Power Semiconductor Devices & ICs*, pp. 130–135, 1992.

[10] A. Schenk, “A model for the field and temperature dependence of Shockley–Read–Hall lifetimes in Silicon, *Solid–Store Electronics*, vol. 35, p. 1585–1596, 1992.